Quantum deflagration and supersonic fronts of tunneling in molecular magnets

D. A. Garanin and Saaber Shoyeb
Department of Physics and Astronomy, Lehman College, City University of New York, 250 Bedford Park Boulevard West, Bronx, New York 10468-1589, USA

Theory of magnetic deflagration taking into account dipolar-controlled spin tunneling has been applied to the realistic model of molecular magnet Mn_{12} Ac. At small transverse field, the front speed v has tunneling maxima on the bias field B_z reflecting those of the molecular spin's relaxation rate calculated from the density-matrix equation. At high transverse field, spin tunneling directly out of the metastable ground state leads to front speeds that can exceed the speed of sound. Both for the weak and strong transverse field, the spatial profile of the deflagration front near tunneling resonances shows a front of tunneling that triggers a burning front behind it.

PACS numbers: 75.50.Xx, 75.45.+j, 76.20.+q

I. INTRODUCTION

Burning or deflagration,[1,2] a self-supporting phenomenon that can exist in the form of propagating fronts, is decay of metastable states, controlled by the temperature increasing as a result of the energy release and heat conduction toward the cold region before the front. The main ingredient of deflagration is the decay rate Γ of the metastable state that has the Arrhenius form $\Gamma = \Gamma_0 \exp[-U/(k_BT)]$ at low temperatures $T \ll U$, where U is the energy barrier. One could ask if deflagration can exist in magnetic systems, many of which are bistable due to a strong uniaxial anisotropy that creates an energy barrier between the two energy minima. However, the energy release in magnetic systems is much weaker than in the case of a regular (chemical) deflagration, thus at room temperatures the ensuing temperature increase is too small to change the relaxation rate and support burning. The situation changes at low temperatures, however, since temperature generated by decay of metastable states can exceed the initial temperature by far and result in a strong increase of Γ. Recently magnetic deflagration has been observed in low-temperature experiments on the molecular magnet Mn_{12} Ac.[3,4] This discovery initiated theoretical[5] and further experimental[6–8] work. Magnetic deflagration has also been observed on manganites.[9] Very fast moving fronts of burning in Mn_{12} Ac initiated by a fast sweep of the magnetic field have been observed in Ref. 10. This leads to the idea of magnetic detonation driven by thermal expansion creating a shock wave.[11,12]

Main exponents of magnetic deflagration, molecular magnets, are built of molecules with a large effective spin, such as $S = 10$ in Mn_{12} and Fe_8. Their uniaxial anisotropy D creates the energy barrier $DS^2 \simeq 67$K for spin rotation[13,14] (see Ref. 15 for a review). Molecular magnets made quite a big splash by the discovery of resonance spin tunneling[16–18] that occurs when spin energy levels on different sides of the barrier match. This is controlled by the bias created by the longitudinal magnetic field. Magnetic molecules in molecular magnets form a crystal lattice (body-centered tetragonal for Mn_{12} Ac). As magnetic cores of the molecules are shielded by organic ligands, there is no exchange interaction between the molecules in the crystal, and the dipole-dipole interaction (DDI) is dominating. Different members of the Mn_{12} family remain in the center of magnetic deflagration research because of the elongated shape of the crystals. To the contrast, Fe_8 crystals have pyramidal shape, inappropriate for studying moving fronts.

The impact of spin tunneling on deflagration in molecular magnets has been addressed in Refs. 4,5,19. Since no transverse magnetic field was applied in experiments so far, tunneling via low-lying states was negligibly small. Thus quantum effects in deflagration could only exist due to thermally assisted tunneling[20,21] via the energy levels just below the top of the barrier. This effect can be taken into account as effective lowering of the barrier U at resonant values of the bias.[22] Peaks of the deflagration front speed vs longitudinal magnetic field (Fig. 4 of Ref. 4) have been interpreted as spin tunneling. The simplest way to explain these peaks was to use the escape rate Γ with the effective barrier U in the standard formula for the speed of the deflagration front, Eqs. (10) and (11) with $\tilde{v} = 1$ (dashed line in Fig. 4 of Ref. 4). For higher bias and thinner crystals, observed speed maxima were much weaker (Fig. 5 of Ref. 6 and Fig. 3 of Ref. 7) that created a controversy.

At the same time, there was a quest for an essentially quantum mechanism of deflagration in molecular magnets that does not reduce to mere barrier lowering in the thermally activated escape rate. As a further development, fronts of spin tunneling (dubbed "cold deflagration") controlled by the dipolar field at zero temperature have been proposed.[23,24] This mechanism requires a strong transverse magnetic field that creates a sufficiently large tunnel splitting Δ between the metastable ground state and an excited state on the other side of the barrier. The idea is that dipolar field created by the sample produces a bias on magnetic molecules (spins) that is typically large in comparison to Δ, thus the dipolar field can control tunneling. As tunneling of one spin changes dipolar fields on other spins, facilitating or preventing their tunneling, the problem is self-consistent. It was shown that there are solutions in which the spatial

distribution of magnetization and dipolar field is adjusting in such a way that there is a moving front of spin tunneling with many spins in the front core being on resonance that allows them to tunnel efficiently. This so-called *laminar* front has been found for not too large values of the external bias. For a larger bias it breaks down, resulting in a slow non-laminar front where most spins are off-resonance.[24] Fronts of cold deflagration exist within the dipolar window of the external bias having the width equal to the dipolar field $B_z^{(D)} = 52.6$ mT produced by a uniformly magnetized molecular magnet.[25,26] In addition to the transverse field, observation of fronts of tunneling in pure form requires a good thermal contact between the crystal and its environment, so that released heat gets conducted away and the temperature remains low.

If the crystal of a molecular magnet is thermally insulated, spin tunneling in a biased case leads to release of Zeeman energy and the temperature increase. In this case both spin tunneling and thermal activation can play a role, so that deflagration is controlled by two parameters, dipolar field and the temperature. The combined quantum-thermal theory of magnetic deflagration has been proposed in Ref. 27. In contrast to the pure cold deflagration, where in the case of overdamped tunneling it is sufficient to use the Lorentzian form of the tunneling rate near the resonance [Eq. (12) of Ref. 24], here one needs the numerically calculated escape rate $\Gamma(B_z, T)$ for both resonant and non-resonant values of B_z. This escape rate has been calculated from the density matrix equation[28] based on the universal spin-phonon interaction.[29,30] To the contrast with the pure cold deflagration that leaves some metastable magnetization unburned behind the front, the combined deflagration leads to complete burning, as the standard magnetic deflagration. This flattens out irregularities of non-laminar fronts and makes them move faster, reaching high speeds at the right end of the dipolar window (see Fig. 4 of Ref. 27).

Ref. 27 used the generic model of a molecular magnet with the anisotropy of the form $-DS_z^2$. In this model, tunneling resonances of all levels take place at the same value of B_z

$$B_z = B_k = kD/(g\mu_B), \qquad k = 0, \pm 1, \pm 2, \dots \tag{1}$$

and, non-trivially, the resonances remain unchanged if transverse magnetic field is applied. In the real Mn_{12} Ac there is an additional term $-AS_z^4$ that makes resonances of different levels be achieved at different values of B_z. The latter was used to experimentally monitor the transition between thermally assisted and ground-state tunneling in Mn_{12} Ac.[31,32] Splitting of tunneling resonances should manifest itself in experiments on magnetic deflagration, and studying related phenomena is one of the aims of this work.

Another aim of this work is to explore the high-speed regime of magnetic burning near the ground-state resonance at high transverse fields. As the speed of fronts of tunneling should be much higher than that of the standard burning fronts driven by heat conduction, burning in these fronts should be independent of the thermal diffusivity, that resembles detonation. To study this regime, more accurate numerical calculations on longer crystals have to be performed.

The rest of the paper is organized as follows. In Sec. II equations describing deflagration with dipolar-controlled spin tunneling are set up and the method of their solution is outlined. Sec. III introduces the relaxation rate of magnetic molecules that is calculated with the help of the density-matrix formalism and contains the effects of both thermal activation and spin tunneling. Sec. IV presents numerical results for the front speed in weak transverse fields. Sec. V is devoted to the case of a strong transverse field, where ground-state tunneling leads to supersonic front speeds. Concluding section summarizes the results obtained and outlines unsolved problems.

II. EQUATIONS OF DEFLAGRATION WITH SPIN TUNNELING AND DIPOLAR FIELD

The system of equation describing deflagration with quantum effects in molecular magnets[27] consists of the rate equation for the metastable population n

$$\frac{\partial n(t,z)}{\partial t} = -\Gamma\left(B_{\mathrm{tot},z}(z), T(z)\right)\left[n(t,z) - n^{(\mathrm{eq})}(T)\right] \tag{2}$$

and the heat conduction equation that can be conveniently written for the thermal energy $\mathcal{E}$ per magnetic molecule

$$\frac{\partial \mathcal{E}(t,z)}{\partial t} = \frac{\partial}{\partial z}\kappa\frac{\partial \mathcal{E}(t,z)}{\partial z} - \Delta E\frac{\partial n(t,z)}{\partial t}. \tag{3}$$

It is assumed that the crystal has an elongated shape and everything depends only on the coordinate z along the geometrical axis of the crystal. The easy axes of magnetic molecules are also directed along this axis, that was the case for all experimentally studied crystals.[3,4,6–8,26] In Eq. (2) $\Gamma(B_z, T)$ is the numerically computed relaxation (escape) rate of magnetic molecules' spins out of the metastable state with the spin pointed to the left, when a longitudinal external field is applied in the direction to the right. $n^{(\mathrm{eq})}(T)$ is the thermal-equilibrium population of the metastable state that is small in the case of a large bias and will be discarded. In Eq. (3) κ is thermal diffusivity that proves to be difficult to measure. Estimations[3] yield $\kappa \sim 10^{-5}\mathrm{m}^2/\mathrm{s}$ (comparable to that of metals) that will be adopted here. The second term in this equation is the source term, in which ΔE is the energy released by transition of one molecular spin from the metastable state to the ground state $|-S\rangle \to |S\rangle$, that is, $\Delta E = 2Sg\mu_B B_z$. The relation between the energy $\mathcal{E}$ and temperature is given by

$$\mathcal{E}(T) = \int_0^T C(T')dT', \tag{4}$$

where $C(T)$ is the experimentally measured heat capacity of Mn_{12}Ac per magnetic molecule.[33]

Since the relaxation rate $\Gamma(B_{\mathrm{tot},z}, T)$ has very sharp maxima at the resonance values of the total longitudinal field $B_{\mathrm{tot},z}$, it is important to include the dipolar field created by the crystal,

$$B_{\mathrm{tot},z}(z) = B_z + B_z^{(D)}(z). \tag{5}$$

Although the dipolar field $B_z^{(D)}$ is much weaker than the external field B_z (and thus can be dropped in ΔE), it is much greater than the width of tunneling peaks in $\Gamma(B_{\mathrm{tot},z}, T)$, so that it can control tunneling. It is convenient to represent $B_z^{(D)}$ in the form

$$B_z^{(D)} = \frac{Sg\mu_B}{v_0} D_{zz}, \tag{6}$$

where D_{zz} is the dimensionless dipolar field, $v_0 = a^2 c$ is the unit-cell volume, a and c are lattice spacings. For Mn_{12} Ac one has $Sg\mu_B/v_0 = 5.0$ mT. For crystals of cylindrical shape with radius R and length L one obtains[25]

$$D_{zz}(z) = \int_0^L dz' \frac{2\pi\nu R^2 \sigma_z(z')}{\left[(z'-z)^2 + R^2\right]^{3/2}} - k_D \sigma_z(z), \tag{7}$$

where ν is the number of molecules per unit cell, $\nu = 2$ for Mn_{12} Ac, $\sigma_z = 1 - 2n$ is polarization of pseudospins representing spins of magnetic molecules ($\sigma_z = \pm 1$ in the ground and metastable states, respectively) and

$$k_D \equiv 8\pi\nu/3 - \bar{D}_{zz}^{(\mathrm{sph})} = 4\pi\nu - \bar{D}_{zz}^{(\mathrm{cyl})} > 0, \tag{8}$$

Here the barred quantities correspond to the reduced dipolar field inside a uniformly magnetized sphere and a long cylinder, and $D_{zz} = \bar{D}_{zz}\sigma_z$ for $\sigma_z = \mathrm{const}$. For Mn_{12} Ac calculations yield[25] $\bar{D}_{zz}^{(\mathrm{sph})} = 2.155$, $\bar{D}_{zz}^{(\mathrm{cyl})} = 10.53$ (in real units $B_z^{(D)} = 52.6$ mT[25,26]), and thus in the local term of Eq. (7) one has $k_D = 14.6$. One can check that Eq. (7) yields the correct result for the field inside a long uniformly magnetized cylinder. At the ends of a cylinder dipolar field has the form $D_{zz} = \left(\bar{D}_{zz}^{(\mathrm{sph})} - 2\pi\nu/3\right)\sigma_z$ that for Mn_{12} Ac becomes $D_{zz} = -2.03\sigma_z$. Dipolar field opposite to the spin orientation is the reason for the instability of the uniformly magnetized state of Mn_{12} Ac that leads to domain formation.[34] For other shapes such as elongated rectangular, one obtains qualitatively similar expressions.[24]

It has to be stressed that the results above represent the dipolar field exactly at the magnetic molecules in the lattice and they depend on the lattice structure. Using the spatially averaged field following from macroscopic magnetostatics would be a mistake. Indeed, the magnetostatic field inside a long uniformly magnetized cylinder is $\mathcal{B}_z^{(D)} = 4\pi M$, where the magnetization is given by $M = \nu S g \mu_B / v_0$. The dipolar field in Mn_{12} Ac is essentially smaller, $B_z^{(D)} = (\bar{D}_{zz}^{(\mathrm{cyl})}/2)M = 5.26M$. The

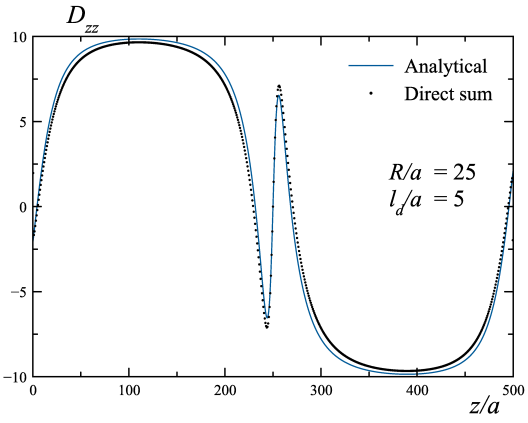

Figure 1: Reduced dipolar field in a deflagration front in the slow-burning limit, created by the magnetization profile $\sigma_z(z) = -\tanh[(z - z_0)/l_d]$. Solid line: Eq. (7); Points: Direct summation of dipolar fields over the Mn_{12} Ac lattice.

difference between the two is due to the local term with k_D in Eq. (7).

A striking feature of Eq. (7) is that the integral and local terms have different signs. The integral term changes at the scale of R while the local term can change faster, that creates a non-monotonic dependence of $D_{zz}(z)$. In the case of a regular magnetic deflagration, the spatial magnetization profile in the slow-burning limit is $\sigma_z(z) = -\tanh[(z - z_0)/l_d]$, where l_d is the width of the deflagration front that satisfies $l_d \ll R$ (see below). The resulting dipolar field is shown in Fig. 1, where the line is the result of Eq. (7) and points represent the dipolar field along the symmetry axis of a long cylindrical crystal calculated by direct summation of microscopic dipolar fields over the Mn_{12} Ac lattice. One can see that Eq. (7) is pretty accurate, small discrepancies resulting from l_d being not large enough in comparizon to the lattice spacing a. The central region with the large positive slope is dominated by the local term of Eq. (7) that changes in the direction opposite to that of the magnetization. For $R \ggg l_d$, D_{zz} reaches the values ± 14.6 due to the local term before it begins to slowly change in the opposite direction. In real units the dipolar field at the local maximum and minimum is $\pm B_z^{(k_D)}$, where

$$B_z^{(k_D)} = 72.9\,\mathrm{mT} \tag{9}$$

exceeding the dipolar field of the uniformly magnetized long cylinder $B_z^{(D)} = 52.6$ mT. Also one can see from Fig. 7 that the dipolar field becomes opposite to the magnetization at the ends of the cylinder, as mentioned above.

Equations (2)–(7) form a system of integro-differential equations describing deflagration with spin tunneling in molecular magnets taking into account the dipole-dipole interaction. Before discussing numerical solution of these equations, it is worth recuperating the results of the stan-

dard ("hot") deflagration and of the cold deflagration. If the whole released energy remains in the body and the initial temperature is very low, the thermal energy per spin behind the front is ΔE. The corresponding temperature defined by the inversion of Eq. (4) is the so-called flame temperature $T_f = T(\Delta E)$ that is in the range 10–15 K in deflagration experiments. Theory of deflagration yields the expressions for the speed of the front v and front width l_d

$$v = \tilde{v}\Gamma_f l_d = \tilde{v}\sqrt{\kappa_f \Gamma_f}, \qquad l_d = \sqrt{\kappa_f/\Gamma_f}, \tag{10}$$

where κ_f and

$$\Gamma_f = \Gamma_0 \exp\left(-W_f\right), \qquad W_f \equiv U/(k_B T_f) \tag{11}$$

are thermal diffusivity and relaxation rate at the flame temperature, while $\tilde{v}$ is a dimensionless coeficient. It was shown[5] that in the slow-burning limit $W_f \gg 1$ one has $\tilde{v} \cong 2/\sqrt{W_f}$. On the other hand, the speed of the laminar front of tunneling at zero temperature is given by[23,24]

$$v = v^* \Gamma_{\rm res} R, \tag{12}$$

where $\Gamma_{\rm res} = \Delta^2/(\hbar^2 \Gamma_{m'})$ is the relaxation rate at overdamped tunneling resonance, $\Delta/\hbar \lesssim \Gamma_{m'}$, $\Gamma_{m'}$ being the decay rate of the matching level m' at the other side of the barrier, R is the width of the crystal (radius of the cylinder in our model), and v^* is a dimensionless coefficient. With a sufficiently strong transverse field applied, one can have $\Delta/\hbar \sim \Gamma_{m'}$ at the applicability limit of the overdamped approximation, and then $\Gamma_{\rm res} \gg \Gamma_f$ because thermal activation goes over high levels of the magnetic molecule where the distances between the levels and thus the energies of phonons involved are much smaller than for the low-lying levels, and also because Γ_f is exponentially small since $T_f \lesssim U$. Additionally, estimation of l_d with $\kappa_f = 10^{-5}\mathrm{m}^2/\mathrm{s}$ and the experimental value $\Gamma_0 = 10^7 \mathrm{s}^{-1}$ yield $l_d \sim 3 \times 10^{-4}$ mm for B_z near the first tunneling resonance and even smaller for larger bias. As in the experiment the width of the crystal was much larger than l_d (0.3 mm in Ref. 3, 0.2 mm in Ref. 6 and 1 mm in Ref. 4), one can see that $\Gamma_{\rm res} R \gg \Gamma_f l_d$ is quite possible in a strong transverse field, and then the front of spin tunneling is much faster than the front of spin burning. A very conservative estimation with $\Gamma_{\rm res} \Rightarrow \Gamma_0 = 10^7$ s^{-1} and $v^* \Rightarrow 1$ for the crystal 0.2 mm thick yields $v \sim 1000$ m/s. As said above, in a strong transverse field one can have $\Gamma_{\rm res} \gg \Gamma_0$, so that the speed of a spin-tunneling front can easily surpass the speed of sound that is about 2000 m/s in molecular magnets (see analysis in Ref. 35). The results of our calculations confirm this.

Discretization of the variable z reduces Eqs. 2, 3, and 7 to a system of ordinary differential equations that can be solved numerically. Very narrow tunneling peaks in $\Gamma(B_z, T)$ make it necessary to carefully control the step in the numerical integration. Wolfram Mathematica's NDSolve proves to be an efficient tool for this problem.

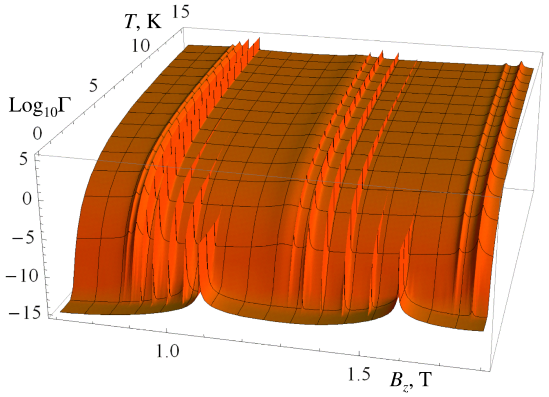

Figure 2: Relaxation rate of Mn_{12}Ac vs temperature and longitudinal magnetic field in the transverse field $B_\perp = 0.04$ T.

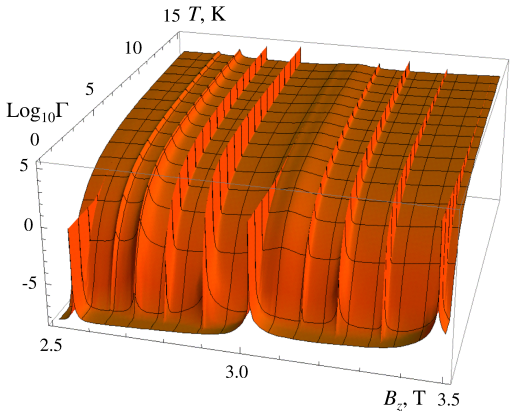

Figure 3: Relaxation rate of Mn_{12}Ac vs temperature and longitudinal magnetic field in the transverse field $B_\perp = 0.04$ T for a stronger bias.

To ignite a deflagration front, the temperature at the left end of the crystal had been increased during a short time. Then the equations were solved and, to find the front speed, the time of arrival of the front at the right end of the crystal was measured.

III. THE RELAXATION RATE

It is crucial to calculate and tabulate the relaxation rate $\Gamma(B_z, T)$ before solving the deflagration problem because a runtime calculation of $\Gamma(B_z, T)$ is practically impossible. We use the effective-spin model with the Hamiltonian containing the uniaxial anisotropy $-DS_z^2 - AS_z^4$ and other anisotropy terms, according to Ref. 36. Spin-phonon interaction is taken into account within the universal model of pure rotations of the crystal field by transverse phonons described in Refs. 29,30,37. Since

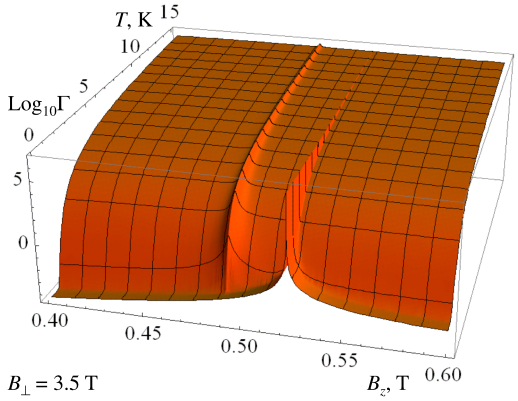

Figure 4: Relaxation rate of $Mn_{12}Ac$ vs temperature and longitudinal magnetic field in the transverse field $B_\perp = 3.5$ T.

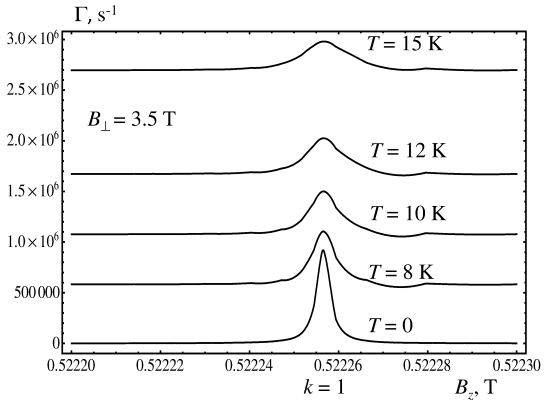

Figure 5: Magnification of the ground-state tunneling peak of $\Gamma(B_z, T)$ (multiplied by 100) at $B_\perp = 3.5$ T.

in this model the crystal field is not distorted, spin-phonon coupling coefficients can be expressed through the measurable crystal-field parameters. The density-matrix equation has been solved within the semi-secular approximation that is valid everywhere, including tunneling resonances.[28]

In the generic model of a molecular magnet with the anisotropy $-DS_z^2$ the fields corresponding to tunneling resonances are given by Eq. (1) for all level pairs. The resulting $\Gamma(B_z, T)$ in a strong transverse field is shown in Fig. 2 of Ref. 27. Tabulation of such a function requires a lot of points along the B_z axis in the vicinity of tunneling maxima. The realistic model with the uniaxial anisotropy $-DS_z^2 - AS_z^4$ is more complicated because tunneling resonances for different level pairs are achieved for different B_z that depend on the transverse field. Thus the first step is to find tunneling peaks numerically for a given transverse field, then to build a non-equidistant grid with a small step near the peaks, then calculate $\Gamma(B_z, T)$ and, finally, make the interpolation. These tasks have been fulfilled with the help of Wolfram Mathematica using a high custom precision and parallelization.

For a weak transverse field (set to $B_\perp = 0.04 - 0.05$ T that may result from a 1° misalignment between the crystal axis and the longitudinal field) $\Gamma(B_z, T)$ contains a zoo of tunneling peaks shown in Fig. 2. The range of B_z here corresponds to that in Ref. 4 and contains groups of resonances with $k = 2, 3$ and partially 4. One can see that ground-state resonances, that are the only survivors at $T = 0$, are achieved at higher fields than resonances of excited states. At temperatures as high as flame temperature, low-lying tunneling resonances are drowned in the non-resonant background. There is also a much weaker non-resonant tunneling at $T = 0$. Relaxation rate at a stronger bias, also in a small transverse field, corresponding to that in Refs. 3,6–8, is shown in Fig. 3. At such bias, the effect of ground-state tunneling begins to appear at high temperatures.

In a strong transverse field such as $B_\perp = 3.5$ T in Fig. 4 the barrier is strongly lowered and most of tunneling resonances are broadened away. Here one can see the ground-state resonance ($B_z = 0.522$), the first-excited-state resonance ($B_z = 0.490$), and with an effort a very broad second-excited-state resonance further to the left. Note the much higher tunneling rate at $T = 0$, in comparison with the previous figure. The range of B_z in Fig. 4 corresponds to the tunneling resonance with $k = 1$. Fig. 5 shows the details of the ground-state peak in Fig. 4. The height and width of this peak increase with temperature. This increase is moderate, however, in comparison to the exponential increase of the non-resonant relaxation rate. The first-excited-state peak in Fig. 4 is higher than the ground-state peak at the flame temperature but is plays a much smaller role in the front propagation, as we will see below.

A long-standing problem in the theory of relaxation of molecular magnets is the prefactor Γ_0 in the Arrhenius relaxation rate being by two orders of magnitude too small. This was already recognized in the early Ref. 21. Without introducing artificially strong spin-phonon interactions,[38] it is impossible to arrive at $\Gamma_0 \sim 10^7 s^{-1}$ observed in experiments[22,33] using the standard spin-lattice relaxation model considering one spin in an infinite elastic matrix. This model could be justified for a strongly diluted molecular magnet but in the normal case it cannot. High density of magnetic molecules should lead to such collective effects as superradiance[39–41] and phonon bottleneck.[42–44] As it would be difficult to deal with these complicated issues while addressing the quantum deflagration problem, the calculated relaxation rate was simply multiplied by 100 to approximately match the experiment. It is instructive to plot the theoretical deflagration speed given by Eq. (10) (with $\tilde{v} = 1$) at small transverse field as function of B_z using the corrected values of $\Gamma(B_z, T_f(B_z))$. Fig. 6 shows a good overall agreement, except for tunneling maxima in the micro-

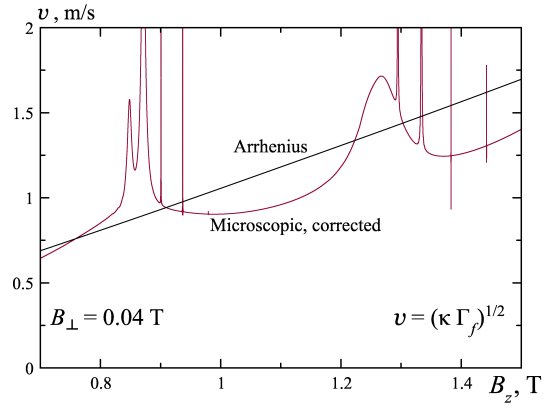

Figure 6: Speed of deflagration front estimated from Eq. (10) for the microscopically calculated relaxation rate $\Gamma(B_z, T_f(B_z))$ with the correction factor 100, together with Eq. (10) using the Arrhenius formula for $\Gamma(B_z, T_f(B_z))$.

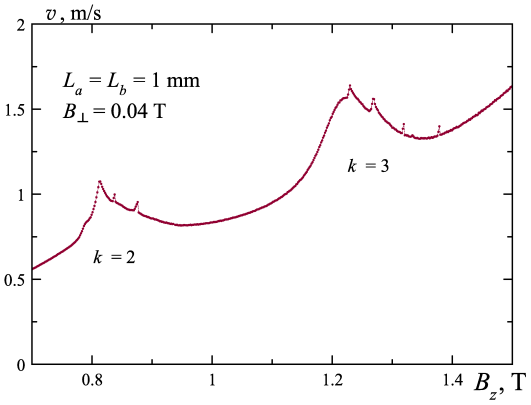

Figure 7: Numerically calculated speed of the deflagration front in a Mn_{12} Ac crystal in small transverse field.

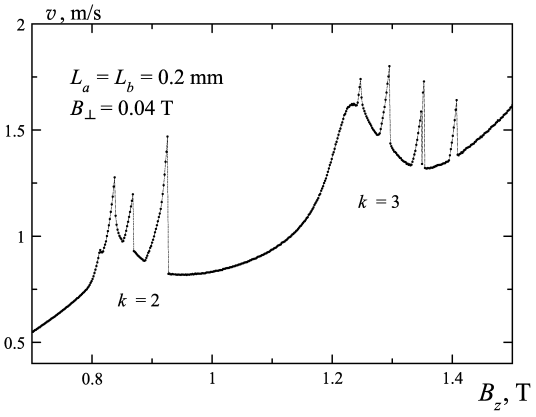

Figure 8: Numerically calculated speed of the deflagration front for small transverse field for a Mn_{12} Ac crystal with a smaller transverse size.

scopically calculated result. As tunneling resonances are broadened by ligand disorder, dipolar field, and nuclear spins, very narrow peaks due to tunneling resonances of lower levels here will be washed out in the experimentally measured front speed. In fact, a similar interpretation of experimental results have been done in Ref. 4, where the dashed line in Fig. 4 is $\sqrt{\kappa_f \Gamma_f}$ with Γ_f taken from relaxation experiments on the same crystal.

An alternative explanation of much higher relaxation rates observed in the experiment is based on deviations from the strong-exchange model that lead to mixing of the states with different total spin S. In Ref. 45 it was shown that this small mixing taken into account perturbatively leads again to the giant-spin model with $S = 10$, however, with additional higher-order crystal-field terms that would normally be absent for d-electrons. These additional terms can explain the observed ground-state tunnel splitting Δ in Fe_8 that is three orders of magnitude larger than the theoretical result using the standard spin Hamiltonian. Similar mechanism could work for Mn_{12} and lead to the increase of the spin-lattice relaxation rate as well. However, the importance of this mechanism is limited to small transverse fields. Most interesting results below for supersonic fronts of tunneling directly out of the metastable ground state without thermal activation require a strong transverse field that produces a large tunnel splitting. In this limit, the latter becomes insensitive to crystal-field terms responsible for tunneling in zero or small transverse fields.

IV. FRONT SPEED AT WEAK TRANSVERSE FIELD

The procedure of numerical solution of the quantum deflagration equations is discussed at the end of Sec. I. The result for the front speed at small transverse fields in the range B_z =0.7–1.7 T is shown in Fig. 7. Here the cylinder radius R in our model has been chosen so that it yields the same cross-section as the crystal of transverse sizes $L_a = L_b = 1$ mm in Ref. 4, that is, $R = \sqrt{L_a L_b/\pi} = 0.564$ mm. One can see that, in comparison to Fig. 6, narrow tunneling peaks are washed out and only broad peaks remain. The reason is that the total magnetic field in the crystal is not constant and changes in the front as shown in Fig. 1, so that tunneling resonances in v are spread. Overall there is a good agreement between our Fig. 2 and Fig. 4 of Ref. 4. For a comparizon, the calculated front speed for a crystal of smaller transverse dimensions, $L_a = L_b = 0.2$ mm, such as in Refs. 6–8 is shown in Fig. 8. In this case tunneling peaks are not washed out, although they are much wider and lower than those in Fig. 6. Some of these peaks are asymmetric, similarly to the single large peak in Fig. 4

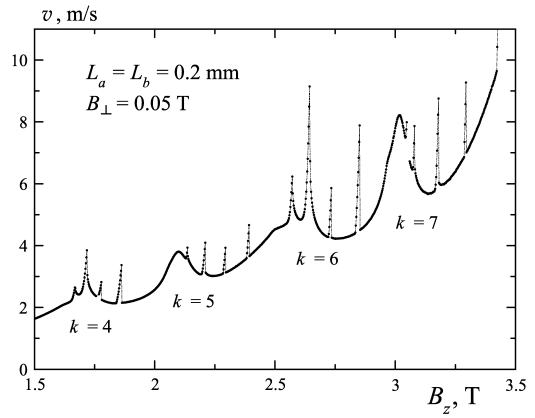

Figure 9: Numerically calculated speed of the deflagration front in a thinner Mn_{12} Ac crystal for small transverse field and a larger bias.

of Ref. 27. The reason for this asymmetry will be discussed below. Then, Fig. 9 shows the calculated front speed for the bias and crystal size corresponding to the experiments in Refs. 6–8. Here tunneling peaks are quite pronounced, at variance with the above experiments that show very small peaks. Just above 3 T and just below 3.5 T there are regions where the speed is too high to be measured in this calculation, an effect of ground-state tunneling.

Spatial profiles of the magnetization, energy, and the total bias field in the deflagration front give an idea of the role played by spin tunneling. Fig. 10 shows these profiles at $B_z = 1.5$ T that is far from resonances. In this case there is a pure slow burning with the magnetization and energy profiles of a tanh shape.[5] Dipolar field shown in the lower panel plays no role in the process.

Fig. 11 shows the spatial profiles at the asymmetric peak of v at $B_z = 2.852$ T in Fig. 9. Here the front speed is high because of tunneling at the face of the front where in the lower panel the total bias field is flat at the level of the tunneling resonance at $B_{z,\mathrm{tot}} = 2.889$ T. Magnetization distribution adjusts so that the dipolar field ensures resonance for a sizable group of spins that tunnel. Tunneling of these spins results in energy release, the temperature and relaxation rate increase, and tunneling gives way to burning in the central and rear areas of the front.

Formation of the asymmetric maxima of the front speed can be explained as follows. When B_z increases, the peak of $B_{z,\mathrm{tot}}$ that arizes due to the local dipolar field reaches the resonant value. Here the strong increase of $v(B_z)$ begins. The maximum of $B_{z,\mathrm{tot}}$ sticks to the resonance value and becomes flat with progressively increasing width. Greater width of the resonance region results in a stronger tunneling and higher front speed. With further increase of B_z, the right edge of the tunneling region moves too far away from the front core into the region where the temperature is too low. As the tunneling resonance in question is thermally assisted, it disappears at low temperatures, thus the flat region of $B_{z,\mathrm{tot}}$ cannot spread too far to the right. As a result, the flat configuration of $B_{z,\mathrm{tot}}$ becomes unstable and suddenly $B_{z,\mathrm{tot}}$ changes to the regular shape of Fig. 1 that crosses the resonance twice in the face part of the front. At the right crossing the temperature is too low and tunneling does not occur, whereas at the left crossing burning already is going on and tunneling cannot add much. There can be the third resonance crossing further to the left but it does not play a role because everything has already burned. It should be noted that multiple resonance crossings do not occur in the laminar regime of the pure quantum case (cold deflagration), see Fig. 2 of Ref. 24.

If the transverse size of the crystal is large, $R \gg l_d$, the slope of $B_{z,\mathrm{tot}}$ to the right of the maximum in Fig. 7 is small. In this case increasing B_z leads to a very quick displacement of the right border of the tunneling region to the right where tunneling cannot take place, as explained above. Thus tunneling peaks of $v(B_z)$ should be very narrow for such crystals. This explains why tunneling peaks are quite pronounced in Fig. 8 but very small in Fig. 7.

Tunneling peaks of $v(B_z)$ corresponding to broad resonances of highly excited states are almost symmetric, such as the high peak at $B_z = 2.644$ T in Fig. 9. In this case peaks are formed when the maximum of $B_{z,\mathrm{tot}}$ crosses the resonance. In these cases progressive flattening of $B_{z,\mathrm{tot}}$ does not occur because here tunneling requires high temperatures and the right border of the tunneling region cannot move to the cold region to the right.

Fig. 12 shows an off-resonance front again, $B_z = 3$ T, but it is not a slow burning front anymore because the bias is high. In this region the analytical theory of Ref. 5 does not work that can be seen on the magnetization and energy profiles that differ from the tanh shape.

V. FRONT SPEED AT STRONG TRANSVERSE FIELD

As one can see from Fig. 4, at strong transverse fields the structure of the relaxation rate $\Gamma(B_z, T)$ simplifies because tunneling resonances of the most excited states broaden away. At $B_\perp = 3.5$ T one can see only two tunneling peaks, and the ground-state tunneling peak is not drowned by the thermal-activation processes up to the highest temperatures. This means that in a bias window around this peak, the barrier is cut completely. The latter changes the dynamics of the system, drastically increasing the role of tunneling in the front propagation. Since tunneling out of the metastable ground state does not require an elevated temperature, the right border of the tunneling region before the main part of the front can shift unlimitedly to the right without causing the instability that kills tunneling, described in the preceding

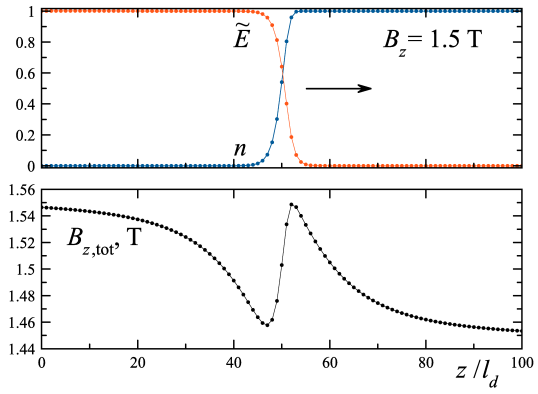

Figure 10: Spatial profiles of the deflagration front in a small transverse field, $B_\perp = 0.05$ T. The bias $B_z = 1.5$T is far from resonances, thus the front is that of a pure slow burning.

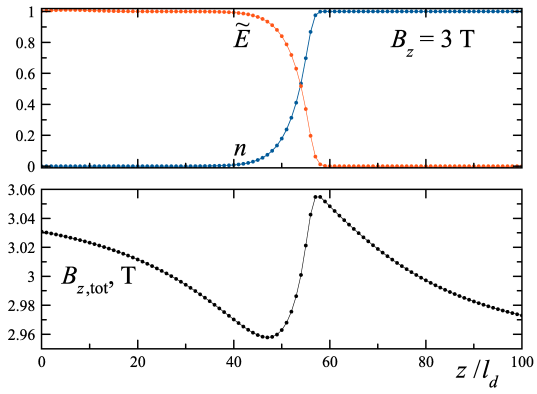

Figure 12: Spatial profiles of the deflagration front in a small transverse field, $B_\perp = 0.05$ T. Faster burning with no tunneling.

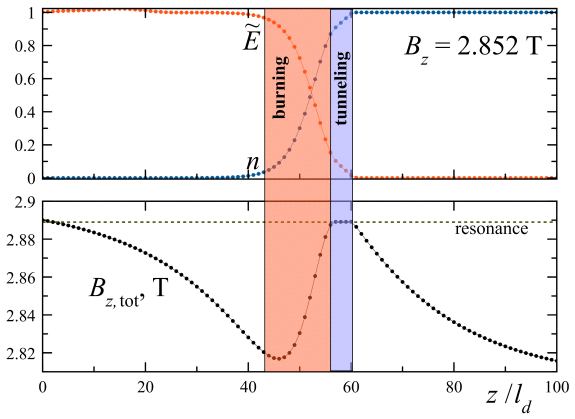

Figure 11: Spatial profiles of the deflagration front in a small transverse field, $B_\perp = 0.05$ T at the peak of the front speed at $B_z = 2.852$ T. There is a resonance spin tunneling at the face of the front and burning in its central and rear parts.

,

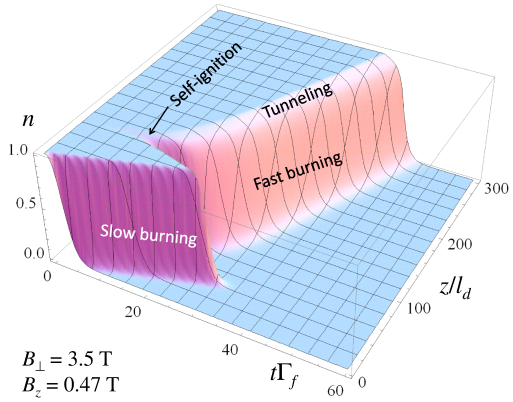

Figure 13: Quantum self-ignition before a slow-burning front, leading to a fast combined tunneling-burning front near ground-state resonance at high transverse fields.

section. Thus the width of the tunneling region can reach the values of order R,[23,24] that leads to front speeds much greater than the speed of a regular magnetic deflagration [see comments after Eq. (12)].

Numerical results at high transverse fields show that shortly after ignition by raising the temperature at the left end of the crystal, a regular slow-burning front can transform into a fast combined tunneling-burning front by *quantum self-ignition* before the slow-burning front, if the crystal is near ground-state tunneling resonance. Fig. 13 shows this phenomenon at $B_\perp = 3.5$ T and $B_z = 0.47$ T, where the ground-state resonance is achieved at $B_{z,\mathrm{tot}} = 0.522$ T. One can see that at short times, $t\Gamma_f \simeq 10$, there is a slow front with a steep profile but before the front, where $B_{z,\mathrm{tot}}$ crosses the resonance value, spins begin to tunnel. This quantum self-ignition leads to flattening of the $B_{z,\mathrm{tot}}$ curve and formation of another, fast moving front, with tunneling followed by burning. The spatial profile of $B_{z,\mathrm{tot}}$ at different times that shows that self-ignition before the slow-burning front is caused by spin tunneling, is shown in Fig. 14.

The front speed v in the vicinity of a biased ground-state resonance in a strong transverse field can achieve supersonic values, as can be seen in Fig. 15. This is in accord with the comments below Eq. (12). To the contrast, the small peak on the left side of Fig. 15 is due to the first-excited-state tunneling resonance at $B_k = 0.490$, see Fig. 4. Its position is given by $B_z = B_k - B_z^{(k_D)} = 0.417$ T that is close to the position in the figure. In Sec. IV it was explaind that front of tunneling via excited levels cannot shift much ahead of the burning zone because it is too cold before the front. This limits the speed of such fronts and explains why the speed of the

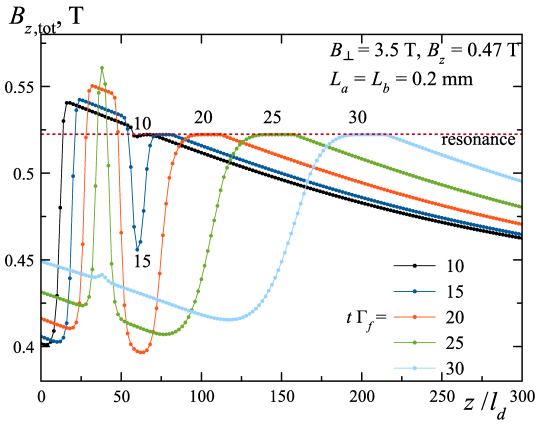

Figure 14: Profiles of the total longitudinal magnetic field at $B_\perp = 3.5$ T and $B_z = 0.47$ T at different moments of time.

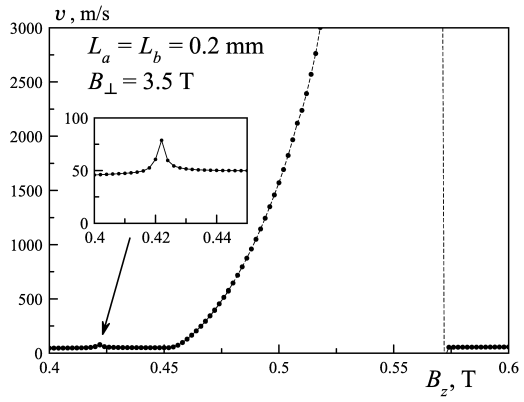

Figure 15: Front speed for a strong transverse field ($B_\perp = 3.5$ T) in the vicinity of the ground-state tunneling resonance at 0.522 T. There is a strong increase of the front speed within the dipolar window of 125.5 mT around the resonance. The small peak on the left (inset) is due to the first-excited-state tunneling resonance.

first-excited state tunneling front is much smaller than that of the ground-state tunneling front, in spite of the relaxation rate at the former being higher.

Returning to the ground-state tunneling front, it should be stressed that no metastable population is left behind the front (see Fig. 13), although there is unburned metastable population behind pure non-thermal fronts of tunneling.[23,24] Here, the metastable population is burning just behind the front of tunneling as the result of the temperature increase. It should be stressed that heat conduction cannot support burning fronts moving faster than the speed of sound and it becomes non-operative in this case. In this respect, the situation is reminding of detonation that has been suggested for molecular magnets in Refs. 11,12 in the case of a strong bias and thus high energy release. In detonation, thermal expansion resulting from burning sends a shock wave into the cold region before the front where, as a consequence, the temperature rises as a result of compression, initiating burning. As the mechanism of detonation is based on elasticity, the speed of a detonation front is comparable to the speed of sound. Fronts of tunneling are not based on elasticity and their speed can be much higher. However, shock waves must accompany tunneling fronts and modify their properties in some way. Experimentally, fast deflagration or detonation fronts in Mn_{12} Ac have been observed in Ref. 10 but they were caused by a very fast sweep of B_z, so that there is a question to which extent the process was self-propelled.

One can see in Fig. 15 that the speed of the front is asymmetric and grows toward the right end of the tunneling window, showing divergence or nearly divergence of the front speed. In the case of cold deflagration (assuming the unbroken laminar regime everywhere) v diverges at the right border of the dipolar window, $B_z = B_k + B_z^{(D)}$, where B_k is the resonance field of Eq. (1). It is given by[24]

$$v \sim \Gamma_{\mathrm{res}} R \frac{B_z - B_k}{B_k + B_z^{(D)} - B_z}, \tag{13}$$

for $B_k \le B_z \le B_k + B_z^{(D)}$, whereas above $B_k + B_z^{(D)}$ it abruptly drops to a zero. The reason for this is that above $B_k + B_z^{(D)}$, the total field well before the front is above the resonance, so that resonance crossing cannot occur. To the contrast, just below $B_k + B_z^{(D)}$ the field well before the front is a little bit below the resonance and increases closer to the front. In this case, there is a wide region where the system is close to the resonance, and the front speed becomes very high. Thus as B_z crosses the value $B_k + B_z^{(D)}$ from below, the front speed drops abruptly. Similar behavior can be seen in Fig. 15: The ground-state resonance is at 0.522 T, and adding the dipolar field $B_z^{(D)} = 0.0526$ T one obtains 0.573 T, as in the figure. However, here v drops to the speed of the regular magnetic deflagration, as also in Fig. 4 of Ref. 27. Another difference is that in the case of cold deflagration[24] tunneling begins at $B_z = B_k$ (left border of the dipolar window) whereas in our case it begins when the local maximum of $B_{z,\mathrm{tot}}$ first touches the resonance (see, e.g., the lower panel of Fig. 11). Since for the crystals studied here the front width is much smaller than the transverse size of the crystal, the dipolar field at the maximum is close to $B_z^{(k_D)}$ given by Eq. (9). Thus the left border of the dipolar window is at $B_z = B_k - B_z^{(k_D)}$, in Fig. 15 at $B_z = 0.45$ T. The total width of the dipolar window of the ground-state tunneling resonance in Mn_{12} Ac is

$$\Delta B_z^{(D)} = B_z^{(D)} + B_z^{(k_D)} = 125.5\,\mathrm{mT} \tag{14}$$

that is much greater than dipolar windows of excited-state tunneling resonances, see, e.g., Fig. 9.

In the case of cold deflagration, there is an unburned metastable population in the final state behind the front, Eq. (41) of Ref. 24 that can be rewritten as

$$n_f = \frac{B_z - B_k}{B_z^{(D)}} \tag{15}$$

($n = 1$ before the front). One can see that the change of n across the front $\Delta n = 1 - n_f$ goes to zero at the right border of the dipolar window $B_k + B_z^{(D)}$. This reconciles the situation with the general requirement that the rate of change of the magnetization of the crystal $\dot{M}$, limited by the tunneling parameter Δ, remains finite. Indeed,

$$\dot{M} \propto (1 - n_f)v = \Gamma_{\rm res} R \frac{B_z - B_k}{B_z^{(D)}} \tag{16}$$

reaches only a finite value $\dot{M} \propto \Gamma_{\rm res} R$ at the right border of the dipolar window before it drops to zero. In the present case of tunneling followed by complete burning, $\dot{M}$ is not limited by Δ and can achieve very high values at the right border of the dipolar window.

VI. DISCUSSION

Numerical calculations for deflagration fronts with dipolar-controlled spin tunneling for the realistic model of Mn_{12} Ac performed in this work have shown many quantum peaks in the dependence of the front speed v on the external magnetic field B_z, if a zero or small transverse field is applied. The multitude of peaks results from the splitting of the tunneling resonance by the $-AS_z^4$ term in the crystal field of the magnetic molecule, and peaks in $v(B_z)$ reflect those in the relaxation rate $\Gamma(B_z, T)$ of the metastable states of Mn_{12} Ac molecules. The peaks of $v(B_z)$ are more pronounced for crystals of a smaller transverse size.

Whereas the results of the calculations for thicker crystals in the range of smaller bias are in a qualitative accord with the experiments of Ref. 4, the results for thinner crystals and stronger bias show much stronger tunneling peaks in $v(B_z)$ than it was observed in Refs. 6–8. One can try to explain the lack of peaks in the experiment by the spread of tunneling resonances as the result of ligand disorder that is pretty strong in Mn_{12} Ac.[46,47] It has been shown that static disorder that is weaker than the dipole-dipole interaction does not destroy fronts of tunneling since the magnetization distribution can adjust so that many spins in the front core are still on resonance and can tunnel.[23] However, static disorder that is stronger than the DDI cannot be accomodated by the latter and should result in spread and suppression of tunneling maxima in $v(B_z)$. The best way to deal with this problem is to make experiments on the members of Mn_{12} family that do not have ligand disorder.

Possibly there is a more fundamental reason for the near absence of tunneling peaks in the experiments of Refs. 6–8. The prefactor Γ_0 in the theoretical relaxation rate being by a factor 10^2 smaller than the measured prefactor suggests collective relaxation processes such as superradiance and phonon bottleneck that can be expected in a dense magnetic system such as molecular magnet. Collective boosting of relaxation processes should not affect tunneling, however. Thus the non-resonant background in $\Gamma(B_z, T)$ can move up by a factor 100, partially drowning tunneling peaks. On the other hand, in our calculation we have boosted the whole function $\Gamma(B_z, T)$, including tunneling peaks.

Whereas it is impossible to develop a collective theory of relaxation in molecular magnets in this paper, one can modify our density-matrix calculation by multiplying spin-phonon coupling amplitudes by 10. This should result in the increase of the non-resonant part of $\Gamma(B_z, T)$ by 100, while one could expect tunneling peaks to be much less changed. Such a calculation has been performed but its results do not show a strong suppression of tunneling peaks in $v(B_z)$. The likely reason for this is that at small transverse field tunneling peaks are due to thermally assisted tunneling that also gets boosted by an artificial increase of spin-phonon interactions.

Calculations in the case of a strong transverse field, making tunneling directly out of the metastable ground state operative, show an increase of the front speed within the tunneling window around the tunneling resonance up to supersonic values. It would be highly interesting to perform experiments on deflagration fronts in this region.

This work has been supported by the NSF under Grant No. DMR-0703639. The author thanks E. M. Chudnovsky for valuable discussions.

[1] I. Glassman, *Combustion* (Academic Press, 1996).
[2] L. D. Landau and E. M. Lifshitz, *Fluid Dynamics* (Pergamon, London, 1987).
[3] Y. Suzuki, M. P. Sarachik, E. M. Chudnovsky, S. McHugh, R. Gonzalez-Rubio, N. Avraham, Y. Myasoedov, E. Zeldov, H. Shtrikman, N. E. Chakov, et al., Phys. Rev. Lett. **95**, 147201 (2005).
[4] A. Hernández-Minguez, J. M. Hernández, F. Macia, A. Garcia-Santiago, J. Tejada, and P. V. Santos, Phys. Rev. Lett. **95**, 217205 (2005).
[5] D. A. Garanin and E. M. Chudnovsky, Phys. Rev. B **76**, 054410 (2007).
[6] S. McHugh, R. Jaafar, M. P. Sarachik, Y. Myasoedov, A. Finkler, H. Shtrikman, E. Zeldov, R. Bagai, and G. Christou, Phys. Rev. B **76**, 172410 (2007).
[7] S. McHugh, B. Wen, X. Ma, M. P. Sarachik, Y. Myasoedov, E. Zeldov, R. Bagai, and G. Christou, Phys. Rev. B **79**, 174413 (2009).

[8] S. McHugh, R. Jaafar, M. P. Sarachik, Y. Myasoedov, A. Finkler, E. Zeldov, R. Bagai, and G. Christou, Phys. Rev. B **80**, 024403 (2009).

[9] F. Macià, A. Hernández-Mínguez, G. Abril, J. M. Hernandez, A. García-Santiago, J. Tejada, F. Parisi, and P. V. Santos, Phys. Rev. B **76**, 174424 (2007).

[10] W. Decelle, J. Vanacken, V. V. Moshchalkov, J. Tejada, J. M. Hernández, and F. Macià, Phys. Rev. Lett. **102**, 027203 (2009).

[11] M. Modestov, V. Bychkov, and M. Marklund, Phys. Rev. B **83**, 214417 (2011).

[12] M. Modestov, V. Bychkov, and M. Marklund, Phys. Rev. Lett. **107**, 20720 (2011).

[13] R. Sessoli, D. Gatteschi, A. Caneschi, and M. A. Novak, Nature (London) **365**, 141 (1993).

[14] A. L. Barra, P. Debrunner, D. Gatteschi, C. E. Schultz, and R. Sessoli, Europhys. Lett. **35**, 133 (1996).

[15] D. Gatteschi, R. Sessoli, and J. Villain, *Molecular Nanomagnets* (Oxford University Press, Oxford, 2006).

[16] J. R. Friedman, M. P. Sarachik, J. Tejada, and R. Ziolo, Phys. Rev. Lett. **76**, 3830 (1996).

[17] J. M. Hernández, X. X. Zhang, F. Luis, J. Bartolomé, J. Tejada, and R. Ziolo, Europhys. Lett. **35**, 301 (1996).

[18] L. Thomas, F. Lionti, R. Ballou, D. Gatteschi, R. Sessoli, and B. Barbara, Nature **383**, 145 (1996).

[19] F. Macià, J. M. Hernandez, J. Tejada, S. Datta, S. Hill, C. Lampropoulos, and G. Christou, Phys. Rev. B **79**, 092403 (2009).

[20] E. M. Chudnovsky and D. A. Garanin, Phys. Rev. Lett. **79**, 4469 (1997).

[21] D. A. Garanin and E. M. Chudnovsky, Phys. Rev. B **56**, 11102 (1997).

[22] F. Luis, J. Bartolomé, J. F. Fernández, J. Tejada, J. M. Hernández, X. X. Zhang, and R. Ziolo, Phys. Rev. B **55**, 11448 (1997).

[23] D. A. Garanin and E. M. Chudnovsky, Phys. Rev. Lett. **102**, 097206 (2009).

[24] D. A. Garanin, Phys. Rev. B **80**, 014406 (2009).

[25] D. A. Garanin and E. M. Chudnovsky, Phys. Rev. B **78**, 174425 (2008).

[26] S. McHugh, R. Jaafar, M. P. Sarachik, Y. Myasoedov, H. Shtrikman, E. Zeldov, R. Bagai, and G. Christou, Phys. Rev. B **79**, 052404 (2009).

[27] D. A. Garanin and R. Jaafar, Phys. Rev. B **81**, 180401 (2010).

[28] D. A. Garanin, in *Advances in Chemical Physics*, edited by S. A. Rice and A. R. Dinner (John Wiley & Sons, Inc., Hoboken, NJ, USA, 2011), vol. 147.

[29] E. M. Chudnovsky, Phys. Rev. Lett. **92**, 120405 (2004).

[30] E. M. Chudnovsky, D. A. Garanin, and R. Schilling, Phys. Rev. B **72**, 094426 (2005).

[31] L. Bokacheva, A. D. Kent, and M. A. Walters, Phys. Rev. Lett. **85**, 4803 (2000).

[32] W. Wernsdorfer, M. Murugesu, and G. Christou, Phys. Rev. Lett. **96**, 057208 (2006).

[33] A. M. Gomes, M. A. Novak, R. Sessoli, A. Caneschi, and D. Gatteschi, Phys. Rev. B **57**, 5021 (1998).

[34] D. A. Garanin, Phys. Rev. B **81**, 220408 (2010).

[35] D. A. Garanin, Phys. Rev. B **78**, 020405(R) (2008).

[36] E. del Barco, A. D. Kent, E. M. Rumberger, D. N. Hendrickson, and G. Cristou, Phys. Rev. Lett. **91**, 047203 (2003).

[37] C. Calero, E. M. Chudnovsky, and D. A. Garanin, Phys. Rev. B **74**, 094428 (2006).

[38] M. N. Leuenberger and D. Loss, Europhys. Lett. **46**, 692 (1999).

[39] R. Dicke, Phys. Rev. **93**, 99 (1954).

[40] E. M. Chudnovsky and D. A. Garanin, Phys. Rev. Lett. **89**, 157201 (2002).

[41] E. M. Chudnovsky and D. A. Garanin, Phys. Rev. Lett. **93**, 257205 (2004).

[42] A. Abragam and A. Bleaney, *Electron Paramagnetic Resonance of Transition Ions* (Clarendon Press, Oxford, 1970).

[43] D. A. Garanin, Phys. Rev. B **75**, 094409 (2007).

[44] D. A. Garanin, Phys. Rev. B **77**, 024429 (2008).

[45] S. Carretta, E. Liviotti, N. Magnani, P. Santini, and G. Amoretti, Phys. Rev. Lett. **92**, 207205 (2004).

[46] K. Park, M. A. Novotny, N. S. Dalal, S. Hill, and P. A. Rikvold, Phys. Rev. B **65**, 014426 (2001).

[47] K. Park, M. A. Novotny, N. S. Dalal, S. Hill, and P. A. Rikvold, Phys. Rev. B **66**, 144409 (2002).